PERGAMON

Mechanism and Machine Theory 37 (2002) 91–113

MECHANISM AND MACHINE THEORY

www.elsevier.com/locate/mechmt

Ball bearing skidding under radial and axial loads

Neng Tung Liao [a], Jen Fin Lin [b,*]

[a] *Department of Mechanical Engineering, National Chinyi Institute of Technology, Taichung 411, Taiwan*
[b] *Department of Mechanical Engineering, National Cheng Kung University, Tainan 701, Taiwan*

Received 31 July 2001; accepted 1 August 2001

Abstract

In the present study, high-speed ball bearings subjected to both axial and radial loads are investigated. This also includes the effect of centrifugal force. Through the geometric analysis of a ball bearing and the force balance, several parameters can be easily obtained, like: the normal forces acting on the contact points; the contact angle at either the inner or the outer raceways that vary with the bearing position angles; bearing stiffness in the axial and radial directions that vary with the cage's angular velocity, etc. Using Hirano's criterion, the conditions for the proper choice of the total deformations in two directions can be identified in order to avoid bearing skidding. The analysis indicates that a more effective way to prevent the bearings from skidding at high angular velocities is to raise the deformation applied in the axial direction. It is the angular velocity of the cage, rather than the load applied in the radial direction that is the dominant factor in the choice of the axial deformation to avoid skidding. © 2002 Published by Elsevier Science Ltd.

Keywords: Ball bearing; Contact angle; Skidding; Centrifugal force; Radial load; Axial load; Stiffness; Deformation

1. Introduction

High-speed angular-contact ball bearings require loading to prevent gross sliding motion, i.e., skidding between the balls and the inner raceway. Skidding occurs when the applied bearing load is inadequate for developing enough elastohydrodynamic tractive force between the raceway and the rolling elements to overcome cage drag, churning losses and prevention of gyroscopic spin. With insufficient tractive force driving the cage assembly at the theoretical epicyclic speed, the inner race must skid past the ball surface. Skidding is therefore gross sliding of the contact surface relative to the opposing surface. Skidding results in surface shear stresses of significant magnitudes in the contact area.

* Corresponding author. Tel.: +886-2757575x6210; fax: +886-06-2352973.
E-mail address: jflin@mail.ncku.edu.tw (J.F. Lin).

0094-114X/02/$ - see front matter © 2002 Published by Elsevier Science Ltd.
PII: S0094-114X(01)00066-0

Nomenclature

A the distance between the raceway groove curvature centers
A^0 the distance between the raceway groove curvature centers under a zero load
d_i the inner raceway diameter
d_m the pitch diameter $(d_i + d_o)/2$
d_o the outer raceway diameter
D the ball diameter
e eccentricity
f_i the dimensionless radius of the groove curvature of the inner raceway; r_i/D
f_o the dimensionless radius of the groove curvature of the outer raceway; r_o/D
F_a the axial load
F_c the centrifugal force
F_r the radial load
g the distance between the bearing center and the curvature center
g_i the distance between the bearing center and the curvature center of the inner raceway
g_o the distance between the bearing center and the curvature center of the outer raceway
h the curvature radius
h_i the curvature radius of the inner raceway
h_o the curvature radius of the outer raceway
K the elastic modulus at the contact point
P_d the bearing diameter clearance
Q_a the axial component of the normal force
Q_i the normal force between the ball and the inner raceway
Q_o the normal force between the ball and the outer raceway
Q_r the radial component of the normal force
r_i the raceway groove curvature radius of the inner raceway
r_o the raceway groove curvature radius of the outer raceway
x the coordinate parallel to the radial load direction
y the coordinate perpendicular to the radial load and the axial direction
z the coordinate in the axial direction
Z the number of balls
α^0 the contact angle under a zero load
α the contact angle
α_i the contact angle of the inner raceway
α_o the contact angle of the outer raceway
δ the elastic deformation
δ_a the total elastic deformation in the axial direction
δ_i the elastic deformation between the ball and the inner raceway
δ_o the elastic deformation between the ball and the outer raceway
δ_r the total elastic deformation in the radial direction
ψ the bearing position angle
ξ_i the coordinate of the center of the inner raceway in the x-direction

ξ_o	the coordinate of the center of the outer raceway in the x-direction
η_i	the coordinate of the center of the inner raceway in the y-direction
η_o	the coordinate of the center of the outer raceway in the y-direction
ζ_i	the coordinate of the center of the inner raceway in the z-direction
ζ_o	the coordinate of the center of the outer raceway in the z-direction
$F(\rho)_i$	the curvature difference of the inner raceway
$F(\rho)_o$	the curvature difference of the outer raceway
$\sum \rho_i$	the curvature sum of the inner raceway
$\sum \rho_o$	the curvature sum of the outer raceway

The comprehensive work that was reported by Jones [1,2] made an important contribution to the kinematics and the dynamics of ball bearings. Various sources of information concerning the contact angles in operating conditions, the forces and moments acting on a ball and the direction of its rolling axis, etc. have been predicted by using his theory. Hirano [3] carried out an experimental investigation on the motion of a ball in an angular-contact ball bearing under thrust load, by measuring the change in magnetic flux induced by a magnetized ball. He found that when the parameter, $Q_a/F_c < 10$ (where Q_a is the axial component of normal force and F_c is the centrifugal force), gross ball slip was observed.

Harris [4] proposed that raceway control is generally valid for high-speed bearings when the traction coefficient at the ball raceway contacts is high enough to prevent any gyroscopic slip. Also, in a later work [5] he pointed out that these simple kinematic hypotheses do not hold up under an elastohydrodynamic traction model, Harris [5] had modified the existing force balance type of analysis to avoid the use of raceway control theories. The convergence of the solution of the non-linear equations is such that a modified quasi-static analysis would strongly depend on the traction-slip characteristics. Boness [6] described the development of an empirical equation used to determine the minimum thrust load that is required to prevent gross ball and cage skidding in high-speed angular-contact bearings. Gupta [7] built equations for the motion of the ball in an angular-contact ball bearing that is operating under elastohydrodynamic traction conditions that are formulated and integrated with prescribed initial conditions. A complete transient and steady state motion is thus obtained to predict the amount of skid and resulting wear rates for a set of given operating conditions. Poplawski et al. [8] serve as a guide to those involved in the selection and evaluation of grease lubricated preloaded angular-contact ball bearings. Detail and discussion were presented regarding the selection of analytical tools, for temperature and load estimation, and use of the correlated model to do parametric studies. The method presented can be applied to the design of other steel and hybrid ball thrust bearing systems.

Most of previous studies on skidding considered only the load in the axial direction and their way of obtaining unknown solutions loads and contact deformations was generally coupled by solving many algebraic equations simultaneously. This study is actually the extension of applying the method that was developed by Liao and Lin [9] to the ball bearing analysis neglecting the centrifugal force. An investigation of high-speed ball bearing subjected to both axial and radial loadings, including the influence of centrifugal force, is conducted. Through the geometric analysis of a ball and force balance, the following parameters can be obtained simply: the total

deformation in either the axial or the radial direction; the mathematical expressions for the curved surfaces of the inner and outer raceways; and the normal and centrifugal forces. If the deformation in both directions and the angular velocity of the cage are given, we can identify the condition without skidding by the plots of the axial deformation versus the radial deformation using Hirano's criterion [3].

By means of this method, the contact angle either at the inner or outer raceways can be obtained easily. Then, the difference in contact angles with the bearing's position angles because of the effect of centrifugal forces at high speeds can be evaluated. Six equations are established six unknowns; however, by proper elimination of five unknowns from these equations, an expression for the unknown α_o (the contact angle at the outer raceway) is given; this equation can then be readily solved numerically. Other unknowns can then be obtained sequentially.

2. Theoretical analysis

The following assumptions are required for the derivation of the contact angle of a ball in a bearing:

1. neither configuration change nor elastic deformation at the inner or outer raceways, except at the ball contact area occur;
2. no thermal effect is considered;
3. friction forces are neglected;
4. no misalignment in the bearing system occurs.

2.1. Contact angle without loading

The geometry of a ball bearing in the absence of load is shown in Fig. 1. The total clearance, P_d, which is the sum of the clearances formed between the ball and the inner raceway and the ball and the outer raceway, is:

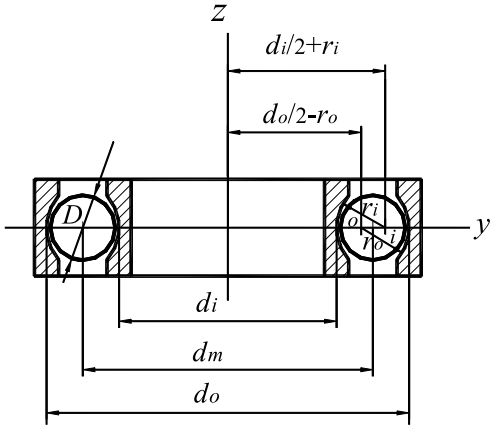

Fig. 1. The cross-section of a single-row ball bearing.

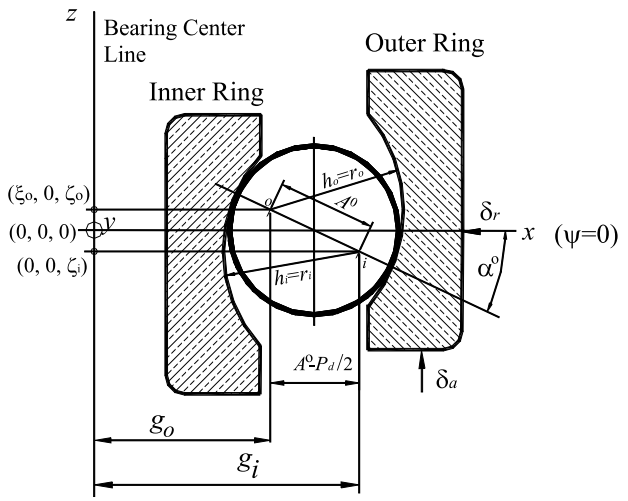

Fig. 2. Cross-section of an unloaded ball bearing that shows the ball-race contacts.

$$P_{\mathrm{d}} = d_{\mathrm{o}} - d_{\mathrm{i}} - 2D, \tag{1}$$

where d_{o} is the diameter of the outer raceway, d_{i} is the diameter of the inner raceway, and D is the ball diameter. As the ball bearing operates under no load, the distance between the two centers of curvature of the inner and outer raceways, as shown in Fig. 2, can be given as

$$A^0 = r_{\mathrm{i}} + r_{\mathrm{o}} - D, \tag{2}$$

where r_{i} is the radius of the curvature of the inner raceway, and r_{o} is the radius of the curvature of the outer raceway. The superscript "0" at the distance A represents no loading. The contact angle under this situation, as shown in Fig. 2, is a constant value, namely [10]

$$\alpha^0 = \cos^{-1}\left(1 - \frac{P_{\mathrm{d}}}{2A^0}\right). \tag{3}$$

2.2. The contact angle under axial and radial loads neglecting the effect of centrifugal force

The radius of curvature of the inner raceway of a ball bearing is r_{i} (equal to h_{i} in Fig. 2), and the entry center of curvature is at point i. Similarly, the radius of curvature center for the outer raceway is r_{o} (equal to h_{o}) and the center of curvature is at point o. Two tori can be formed for the inner and outer raceways, respectively.

Each of these two tori is generated by a circle with either r_{i} or r_{o} as radius, and point i or point o as center; then, by rotating this circle around the passing through the point of coordinates (ξ, η, ζ). The general diagram for the torus generated for either the inner or the outer raceways is shown in Fig. 3. Apparently, the coordinates for the geometric center of these two tori are different, and are dependent upon the loading condition. In the case of a ball bearing before a loading, the geometric center of the torus of the outer raceway is located at the point of coordinates $(0, 0, \zeta_{\mathrm{o}})$, whereas the one for the torus of the inner raceway has the coordinates $(0, 0, \zeta_{\mathrm{i}})$. As the bearing is

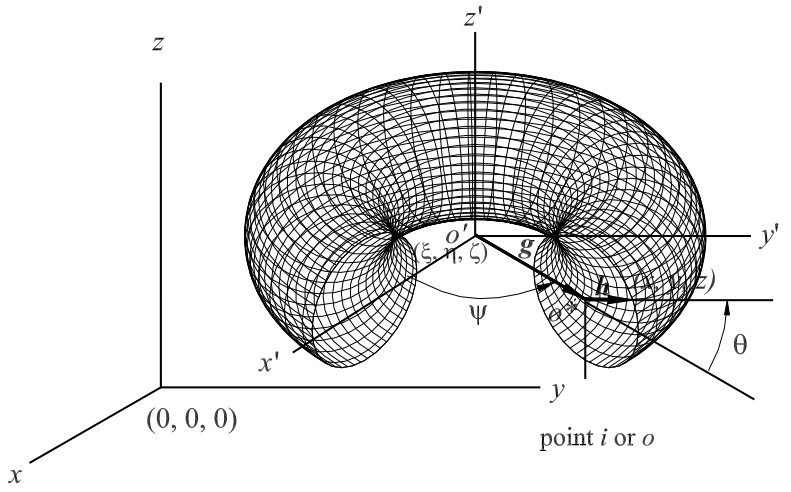

Fig. 3. Two coordinate systems and the torus produced by one of two raceways in a ball bearing.

loaded, the geometric center of the torus of the inner raceway remains unchanged because the inner raceway is fitted tightly with the rotating shaft and the radius of curvature is assumed to be unchanged even under loading. However, the geometric center of the torus corresponding to the outer raceway is now moved to $(\xi_o, 0, \zeta_o)$. From the geometry of Figs. 2 and 4, the coordinates of any point on the surface of the inner raceway can be written as

$$\begin{aligned}(x_i, y_i, z_i) &= (\xi_i, \eta_i, \zeta_i) + g_i(\cos\psi, \sin\psi, 0) + h_i(\cos\theta\cos\psi, \cos\theta\sin\psi, \sin\theta),\\ &= (0, 0, \zeta_i) + g_i(\cos\psi, \sin\psi, 0) + h_i(\cos\theta\cos\psi, \cos\theta\sin\psi, \sin\theta),\end{aligned} \tag{4}$$

where

$$g_i = d_i/2 + r_i \tag{5a}$$

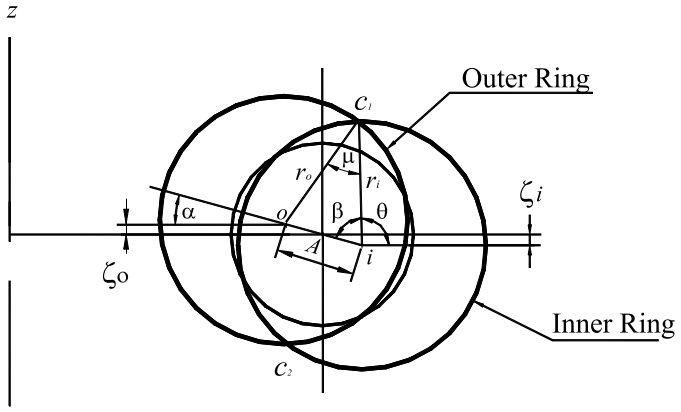

Fig. 4. A ball in contact with the outer and inner rings under the loads that are in the radial and axial direction.

and

$$h_i = r_i. \tag{5b}$$

The subscript i of all parameters denotes association with the inner raceway, and ψ is the position angle on the x'–y' plane, and since $\xi_i = \eta_i = 0$, Eq. (4) can now be written as

$$(x_i, y_i, z_i) = ((g_i + h_i \cos\theta)\cos\psi, (g_i + h_i \cos\theta)\sin\psi, h_i \sin\theta + \zeta_i), \tag{6}$$

where ζ_i in Eq. (6), as Fig. 4 shows, is given by

$$\zeta_i = -\left(r_i - \frac{D}{2}\sin\alpha^o\right). \tag{7}$$

In Eq. (7), r_i is the radius of curvature of the inner raceway and α^0 is the ball's contact angle under zero load. Here, the contact angles of the ball at the inner raceway and the outer raceway are assumed to be the same, provided that the centrifugal force acting on the ball is ignored. Similarly, the coordinates for any one point on the outer raceway surface, as shown in Fig. 2, are given as:

$$(x_o, y_o, z_o) = (\xi_o, \eta_o = 0, \zeta_o) + g_o(\cos\psi, \sin\psi, 0) + h_o(\cos\theta\cos\psi, \cos\theta\sin\psi, \sin\theta), \tag{8}$$

where

$$g_o = d_o/2 - r_o \tag{9a}$$

and

$$h_o = r_o. \tag{9b}$$

The bearing elastic deformation produced in the x-direction due to the externally applied radial load is δ_r; and the total elastic deformation in the z-direction (parallel to shaft axis) is δ_a due to the externally applied axial load. Then, the coordinates ξ_o and ζ_o in Eq. (8) are given by

$$\xi_o = -\delta_r, \tag{10a}$$

$$\zeta_o = (r_o - D/2)\sin\alpha^0 + \delta_a. \tag{10b}$$

The two elastic deformations, δ_r and δ_a, are given in this study because they can be readily obtained from the experimental measures by the use of the displacement gauge. Then Eq. (8) can be rewritten as:

$$(x_o, y_o, z_o) = ((g_o + h_o \cos\theta)\cos\psi + \xi_o, (g_o + h_o \cos\theta)\sin\psi, h_o \sin + \zeta_o). \tag{11}$$

The two tori which have point i and point o as the center of two circles and r_i and r_o as the radius of these two circles for the inner and outer raceways, respectively, the points of intersection of the cross-sections of two tori are c_1 and c_2. According to Fig. 4, the contact angle α can be written as:

$$\alpha = \pi - \theta - \beta. \tag{12}$$

This contact angle is the same in the inner and the outer raceways if the centrifugal force is ignored. The angle β shown in Fig. 4, by the sine theorem, is given as:

$$\frac{\sin\beta}{r_o} = \frac{\sin\mu}{A}. \tag{13}$$

Then, angle β is obtained as:

$$\beta = \sin^{-1}\left(\frac{r_o \sin\mu}{A}\right), \tag{14}$$

where A is the distance between the two centers of curvature i and o obtained as the bearing loaded. Based on the cosine theorem, the angle μ satisfies the expression:

$$\cos\mu = \frac{r_i^2 + r_o^2 - A^2}{2r_i r_o} \tag{15}$$

or

$$\sin\mu = \sqrt{1 - \left(\frac{r_i^2 + r_o^2 - A^2}{2r_i r_o}\right)^2}. \tag{16}$$

Substituting Eq. (16) into Eq. (14), we can obtain the following expression:

$$\beta = \sin^{-1}\left(\frac{r_o}{A}\sqrt{1 - \left(\frac{r_i^2 + r_o^2 - A^2}{2r_i r_o}\right)^2}\right). \tag{17}$$

In most practical applications, the bearing has the same radius of curvature for both the inner and the outer raceways ($r_o = r_i$). Consequently, Eq. (17) can be further simplified as (shown in Fig. 4):

$$\beta = \sin^{-1}\sqrt{1 - \left(\frac{A}{2r_o}\right)^2} \tag{18}$$

or

$$\beta = \cos^{-1}\left(\frac{A}{2r_o}\right). \tag{19}$$

According to Eq. (12), the contact angle α can be obtained only when the angle θ is available. The angle θ can be solved as follows.

The angles θ and ψ in Eq. (11) are now temporarily replaced by u and v, respectively; then, Eq. (11) can be rewritten as:

$$x_o = (g_o + h_o\cos u)\cos v + \xi_o = (g_o + h_o\cos u)\cos v - \delta_r, \tag{20a}$$

$$y_o = (g_o + h_o\cos u)\sin v, \tag{20b}$$

$$z_o = h_o\sin u + \zeta_o. \tag{20c}$$

The intersections of the cross-sections of two tori must satisfy

$$(g_i + h_i\cos\theta)\cos\psi = (g_o + h_o\cos u)\cos v - \delta_r, \tag{21a}$$

$$(g_i + h_i\cos\theta)\sin\psi = (g_o + h_o\cos u)\sin v, \tag{21b}$$

$$h_i\sin\theta + \zeta_i = h_o\sin u + \zeta_o. \tag{21c}$$

We will isolate $h_o\sin u$ in Eq. (21c)

$$h_o\sin u = h_i\sin\theta + \zeta_i - \zeta_o. \tag{22}$$

And we can obtain Eq. (23) from Eq. (22)

$$h_o \cos u = \sqrt{h_o^2 - (h_i \sin\theta + \zeta_i - \zeta_o)^2}. \tag{23}$$

Now square both sides of Eq. (21a) and (21b) and add them for eliminating the variable v:

$$[(g_i + h_i \cos\theta)\cos\psi + \delta_r]^2 + [(g_i + h_i \cos\theta)\sin\psi]^2 = (g_o + h_o \cos u)^2. \tag{24}$$

Substituting Eq. (23) into Eq. (24), the variable u can be eliminated from Eq. (24), the angle θ thus satisfying:

$$(g_i + h_i \cos\theta)^2 + 2\delta_r(g_i + h_i \cos\theta)\cos\psi + \delta_r^2 - \left[g_o + \sqrt{h_o^2 - (h_i \sin\theta + \zeta_i - \zeta_o)^2}\right]^2 = 0. \tag{25}$$

The solutions of θ in Eq. (25) are dependent upon the position angle ψ; that is, the contact angle α varies with the position angle of a ball bearing. The above equation can be solved by a Newton method if the bearing elastic deformations in radial and axial direction, δ_r, δ_a, are available. If the angle θ is obtained, the contact angle α is thus achievable from Eq. (12). In Eq. (19), the distance A between the two centers of curvature i and o is calculated as follows:

$$\begin{aligned} A &= \|((g_o \cos\psi - \delta_r, g_o \sin\psi, \zeta_o) - (g_i \cos\psi, g_i \sin\psi, \zeta_i))\|, \\ &= \|((g_o - g_i)\cos\psi - \delta_r, (g_o - g_i)\sin\psi, \zeta_o - \zeta_i)\|, \\ &= \left\{[(g_o - g_i)\cos\psi - \delta_r]^2 + [(g_o - g_i)\sin\psi]^2 + (\zeta_o - \zeta_i)^2\right\}^{1/2}. \end{aligned} \tag{26}$$

2.3. The contact angles of the inner and the outer raceways in the presence of centrifugal forces

The contact angle at the inner and the outer raceways is variable. It varies depending upon the bearing angular velocity. Define the change in contact at the inner and outer raceways as:

$$\Delta\alpha_i = \alpha_i - \alpha, \tag{23a}$$

$$\Delta\alpha_o = \alpha - \alpha_o, \tag{23b}$$

where α is the contact angle of a bearing under loading but without taking centrifugal forces into account; α_i and α_o are the real contact angles at the inner and the outer raceways, respectively, but considering centrifugal forces. The above angle differences are not equal because the contact angle α_i is in general different from α_o if centrifugal forces are included. Then, a triangle *moi* is formed as shown in Fig. 5, where point m is the center of the ball that is tangent to both the inner and the outer raceways tori the absence of elastic deformations at these two contact points. If the radius of curvature of the inner and the outer raceways is assumed to be equal to r, then

$$r_i = r_o = r \tag{27}$$

and the angle differences $\Delta\alpha_i$ and $\Delta\alpha_o$ are approximately

$$\Delta\alpha_i \cong \Delta\alpha_o \cong \Delta\alpha. \tag{28}$$

Let the distance between point i and point o ($\overline{io}$) be A, the distance between point i and point m ($\overline{im}$) be B, the distance between point o and point m ($\overline{om}$) be C. Then B and C, as shown in Fig. 5, can be expressed as

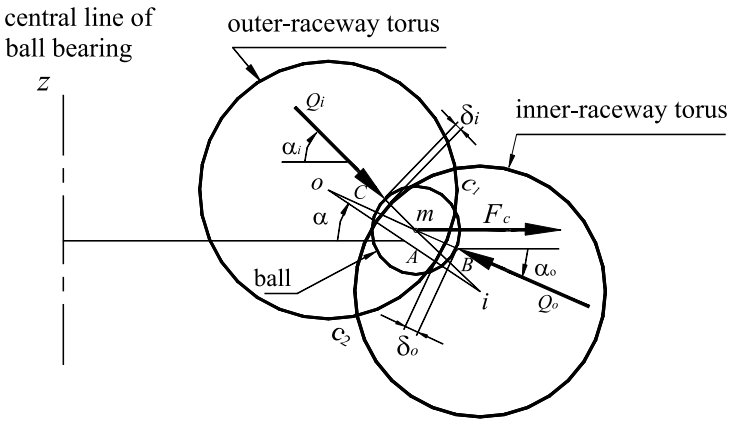

Fig. 5. The ball-raceway contacts under loading in the axial and radial directions and the ball's centrifugal force.

$$B = r_{\mathrm{i}} + \delta_{\mathrm{i}} - \frac{D}{2} = r + \delta_{\mathrm{i}} - \frac{D}{2}, \tag{29a}$$

$$C = r_{\mathrm{o}} + \delta_{\mathrm{o}} - \frac{D}{2} = r + \delta_0 - \frac{D}{2}, \tag{29b}$$

where δ_{i} and δ_{o} are the elastic deformations arising at the contact point of the inner and the outer raceways, respectively. The distances B and C also satisfy

$$C^2 = A^2 + B^2 - 2AB\cos(\Delta\alpha), \tag{30a}$$

$$B^2 = A^2 + C^2 - 2AC\cos(\Delta\alpha). \tag{30b}$$

Eliminating B and C from Eqs. (29a)–(30b) gives

$$(2r - D + \delta_{\mathrm{i}} + \delta_{\mathrm{o}})\cos(\Delta\alpha) = A. \tag{31}$$

If the frictional forces produced at the ball are so small that they are excluded from the force balance, the equations of the force balance in the y- and z-direction are as shown in Fig. 5, namely,

$$Q_{\mathrm{i}}\sin\alpha_{\mathrm{i}} - Q_{\mathrm{o}}\sin\alpha_{\mathrm{o}} = 0, \tag{32a}$$

$$Q_{\mathrm{i}}\cos\alpha_{\mathrm{i}} - Q_{\mathrm{o}}\cos\alpha_{\mathrm{o}} + F_{\mathrm{c}} = 0, \tag{32b}$$

where the centrifugal force F_{c} in Eq. (32b) due to high angular velocities can be written as

$$F_{\mathrm{c}} = \frac{d_{\mathrm{m}}}{2} m\omega_{\mathrm{c}}^2, \tag{33}$$

where m is the mass of the ball; d_{m} is the bearing pitch diameter; and ω_{c} is the angular velocity of the cage. The normal contact force at the inner raceway, can be decided from Eq. (32a), as

$$Q_{\mathrm{i}} = \frac{\sin\alpha_{\mathrm{o}}}{\sin\alpha_{\mathrm{i}}} Q_{\mathrm{o}}. \tag{34}$$

If the elastic deformation of the contact point at either the inner or the outer raceways is available, the normal contact force at the inner and the outer raceways can be stated as

$$Q_i = K_i \delta_i^{1.5}, \tag{35a}$$

$$Q_o = K_o \delta_o^{1.5}, \tag{35b}$$

where the elastic moduli, K_i and K_o, in the above two equations can be obtained as shown in Appendix A. Substituting Eqs. (35a) and (35b) in Eq. (34) gives

$$K_i \delta_i^{1.5} = \frac{\sin \alpha_o}{\sin \alpha_i} K_o \delta_o^{1.5}. \tag{36}$$

Substitution of Eqs. (34) and (35b) into Eq. (32b) gives

$$\left(\frac{\sin \alpha_o}{\tan \alpha_i} - \cos \alpha_o \right) K_o \delta_o^{1.5} + F_c = 0. \tag{37}$$

Eq. (36) can be rewritten as

$$\delta_i = \left(\frac{K_o \sin \alpha_o}{K_i \sin \alpha_i} \right)^{2/3} \delta_o. \tag{38}$$

Elimination of $\Delta\alpha_i$ from Eqs. (23a) and (23b) gives

$$\alpha_i + \alpha_o = 2\alpha. \tag{39}$$

Substituting Eqs. (38) and (39) into Eq. (31) gives

$$\left\{ 2r - D + \left[\left(\frac{K_o \sin \alpha_o}{K_i \sin(2\alpha - \alpha_o)} \right)^{2/3} + 1 \right] \delta_o \right\} \cos(\alpha - \alpha_o) - A = 0. \tag{40}$$

Eliminating δ_o from Eq. (40) specify using Eq. (37) gives the above equation as a function of α_o. Then, it can be solved by a Newton method. The other unknowns α_i, Q_i, Q_o and δ_i are thus obtained from Eqs. (39), (32a), (32b) and (35a). The summation of the load components for a bearing with Z balls gives the total load (see Fig. 6) in the axial direction as:

$$F_a = \sum_{j=1}^{Z} Q_{aj}, \tag{41a}$$

where j denotes jth ball bearing;

$$Q_a = Q_i \sin \alpha_i$$

and for the total load in the radial direction can be written as:

$$F_r = \sum_{j=1}^{Z} Q_{rj} \cos \psi, \tag{41b}$$

where

$$Q_r = Q_i \cos \alpha_i.$$

2.4. The criteria for the skidding threshold

Hirano [3] carried out several experiments to investigate the gross ball slip occurring in ball bearings under various operating conditions and tried to induce the threshold of bearing skidding from experimental results. The criterion for bearing skidding is stated as:

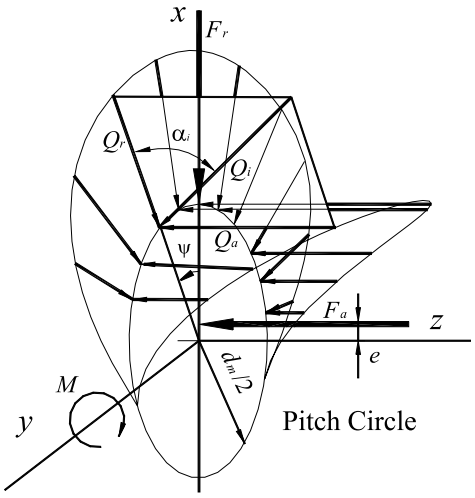

Fig. 6. Moment and load distribution of the pitch circle in a ball bearing under a combined radial and axial loads.

$$\frac{F_c}{Q_a} \geqslant 0.1 \text{ or } \frac{Q_a}{F_c} \leqslant 10. \tag{42}$$

If this inequality is true, then skidding between ball and inner raceway will occur. This criterion deduced by Hirano was from the investigation of many experiments on ball bearings.

3. Results and discussion

3.1. The contact angle at the inner and the outer raceways

The contact angles at the inner and the outer raceways vary with the position angle of a b218 angular-contact ball bearing, as shown in Fig. 7. The dimensions of this bearing are shown in Table 1. Axial and radial deformations are applied with the same value of 0.01 mm. In the static case, the centrifugal force of the balls in a bearing is neglected. If the centrifugal force is considered at high angular velocities, either the inner or the outer contact angle varies with the bearing position angle ψ and the angular velocity ω_c of the cage. At the inner raceway, the maximum contact angle is formed at an angle of 180° from the x-axis (the radial direction). At the outer raceway, the minimum contact angle is also formed at the same bearing position. The contact angle at the inner raceway is increased by increasing the angular velocity of the cage. Conversely, the contact angle at the outer raceway diminishes by increasing the angular velocity of the cage. The difference in the contact angle between the inner and outer raceways is enlarged by increasing the cage's angular velocity ω_c.

The variations of the load in either the axial or the radial direction are shown in Fig. 8 as functions of cage's angular velocity. If these two deformations are fixed, the axial load applied to the system is close to linearly related to the cage's angular velocity. However, the radial load declines to the minimum value as the cage's angular velocity reaches around 8000 rpm, then

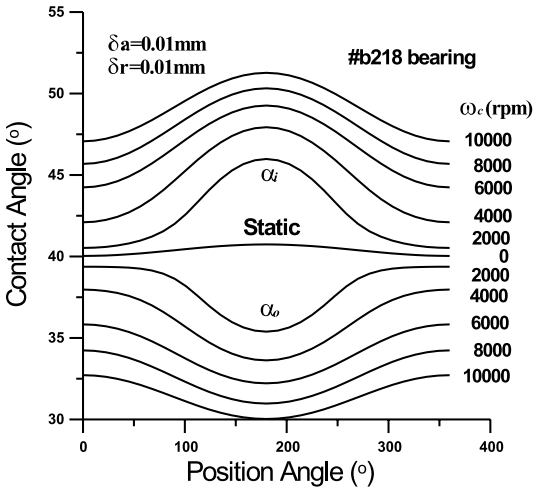

Fig. 7. The contact angle at either the inner or outer raceway varying with the bearing position angle for different cage's angular velocities.

Table 1
The dimensions of the b218 and #7307 angular-contact ball bearing

Bearing type	Contact angle α^0	Z	r_i (mm)	r_o (mm)	d_i (mm)	d_o (mm)	D (mm)
b218	40.0°	16	11.6281	11.6281	102.7938	147.7264	22.225
#7307	39.4°	11	7.0500	7.0500	43.8110	71.0680	13.491

Z: ball number.

further increase in the cage's angular velocity causes an increase in the radial load. There exists an extreme value for the radial load at certain cage speeds. Substitution of Eq. (33) into Eq. (32b) gives the radial contact force at bearing position angle ψ as

$$\begin{aligned} Q_r &= Q_i \cos\alpha_i, \\ &= Q_o \cos\alpha_o - \frac{d_m}{2} m\omega_c. \end{aligned} \tag{43}$$

Since the radial load F_r of a ball bearing, as shown in Eq. (41b) is obtained then Q_r is available. Taking the partial derivative of the radial load F_r with respect to the cage's angular velocity ω_c gives

$$\begin{aligned} \frac{\partial F_r}{\partial \omega_c} &= \sum \frac{\partial Q_r}{\partial \omega_c} \cos\psi \\ &= \sum \left(\frac{\partial}{\partial \omega_c} (Q_o \cos\alpha_o - d_m m\omega_c^2/2) cos\psi \right) \\ &= \sum \frac{\partial}{\partial \omega_c} (Q_o \cos\alpha_o) \cos\psi - \sum d_m m\omega_c \cos\psi. \end{aligned} \tag{44}$$

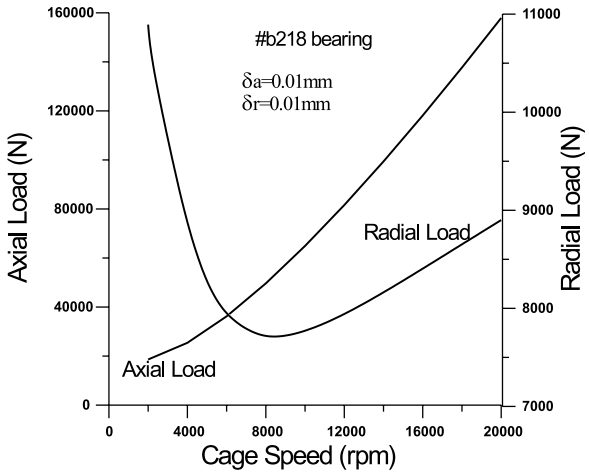

Fig. 8. Axial and radial loads varying with the cage's angular velocity under deformations of $\delta_a = 0.01$ mm and $\delta_r = 0.01$ mm.

The first term on the right-hand side of Eq. (44) represents the summation of all the components in x-direction of the normal forces acting upon the balls. The second term denotes the summations of all components in x-direction of all centrifugal forces acting upon the balls. If $\partial F_r/\partial \omega_c = 0$, an extreme value of F_r exists; i.e., the first term is of magnitude equal to the second term. This is found at a cage's angular velocity of about 8000 rpm.

3.2. The normal force acting upon the inner and the outer raceways

The normal forces at various angular velocities of the cage acting at the contact points of either the inner or the outer raceways are shown in Fig. 9. The curve marked "static" is obtained in the absence ball's centrifugal force. The area near the position angle of 180° does not have a normal force acting upon either the inner or the outer raceways. This feature mainly results when the balls rolling on this area are separated from the inner raceway such that the normal forces acting on the inner and the outer raceways are nearly zero. This separation can be avoided when taking the balls' centrifugal force into account in the analysis. The normal force at the position angle of 180° from the radial load direction is a minimum, irrespective of the inner or the outer raceways. The normal force acting upon the outer raceway is still higher than that upon the inner raceway, and an increase in the cage's angular velocity magnifies the difference between these two loads.

Generally speaking, the normal force acting on either the inner or the outer raceways is governed by the combined effect of the ball's centrifugal force and the contact angle at the two raceways. They both are actually determined by the cage's angular velocity. Increasing the cage's angular velocity will enhance the ball's centrifugal force. On the other hand, the cage's angular velocity will increase the contact angle at the inner raceway and decrease the contact angle at the outer raceway. The variations in both of the contact angles will lead to a decline of the normal force acting at the contact point when the cage's angular velocity is increased. The combined effects according to the force diagram shown in Fig. 5 cause the normal force acting on the outer

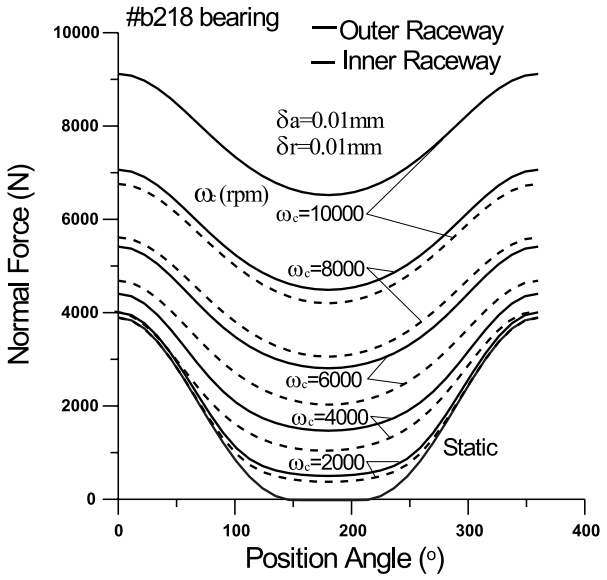

Fig. 9. The normal forces acting on the inner and outer raceways vs. the bearing position angle for deformations of $\delta_a = 0.01$ mm and $\delta_r = 0.01$ mm at different cage's angular velocities.

raceway to be noticeably higher than that acting on the inner raceway when the cage's angular velocity is sufficiently high.

Fig. 10(a) shows the contact angles, α_i and α_o varying at the cage's angular velocity ω_c, under various axial loads when no radial load is applied ($\delta_r = 0$). The area on the right-hand side of the curve is marked "Δ" and denotes the contact angles formed in a bearing by applying a positive axial deformation ($\delta_a > 0$). In this area, the contact angle at the inner raceway α_i is increased if a non-zero δ_a is applied by raising the load in the axial direction, whereas the contact angle at the outer raceway α_o is decreased, irrespective of the angular velocity of the cage ω_c. Increasing the cage's angular velocity would increase the inner contact angle α_i, but would decrease the outer contact angle α_o when the axial load is fixed. When the angular velocity of the cage is low, the increase in the axial load makes α_i and α_o quite close.

The area between the two dash lines points out the combined conditions of the axial deformation δ_a and the cage's angular velocity such that surface skidding can be avoided in the b218 bearing system. It is the cage's angular velocity, rather than the axial deformation, that is the primary controlling factor on surface skidding. Surface skidding can be inhibited only when the cage's angular velocity is considerably lowered and there is an appropriate high axial load applied to the system. Fig. 10(b) shows the contact angles at the inner and outer raceways varying with the radial load. The axial deformation is fixed at 0.01 mm, and the radial deformation is varied in the range 0.001–0.01 mm. Since a non-zero radial load applied to the bearing would cause the load distributions to be non-symmetric with respect to the axis, the contact angles α_i and α_o vary with the bearing position angle ψ. The plots in this figure are shown as $\psi = 0$. Either of the contact angles α_i or α_o is expressed as a function of the cage's angular velocity and the radial load. However, it is the cage's angular velocity that is the primary controlling factor for the two contact

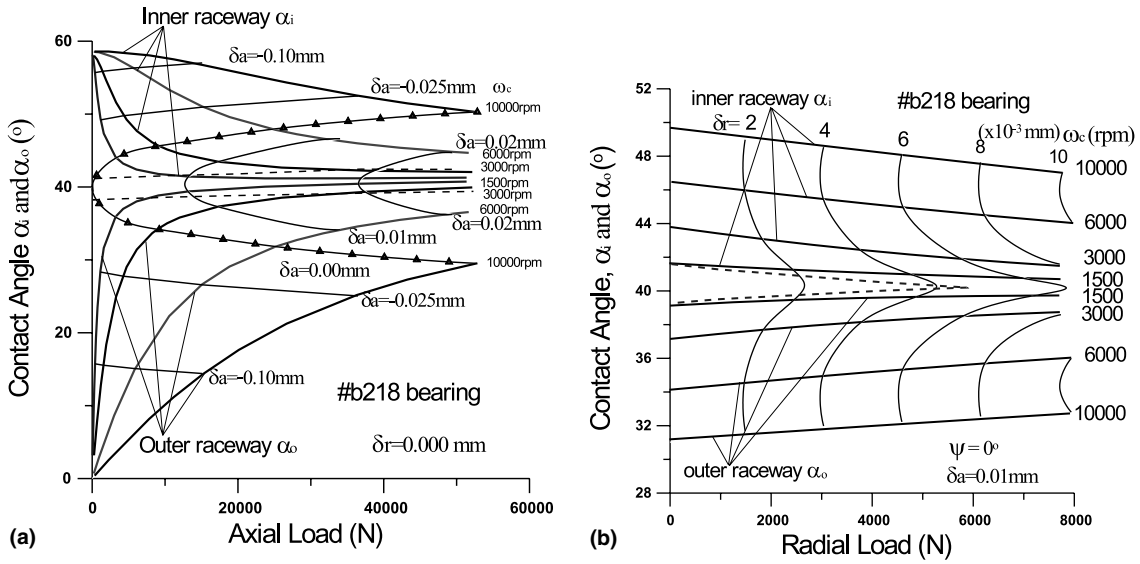

Fig. 10. (a) Contact angles α_i and α_o varying with the thrust load in the axial direction of $\delta_r = 0$ mm at different cage's angular velocity; (b) contact angles α_i and α_o varying with radial load of $\delta_a = 0.01$ mm at $\psi = 0°$ for different cage's angular velocities.

angles. Similarly, the area outside the dash lines indicates the conditions that cause skidding. Surface skidding seems unavoidable at various angular velocities of the cage because the current combinations of δ_r and δ_a cannot satisfy the criterion of $Q_a/F_c > 10$.

3.3. The skidding region

According to the criterion shown in Eq. (42) for skidding, the threshold can be expressed as a function of the deformations applied in both the axial and the radial directions. Fig. 11 shows the threshold for skidding can be expressed by a straight line in the plot of axial deformation versus radial deformation. In the subregion above the threshold line, bearing skidding can be avoided by applying the proper deformations in the two directions of the bearings that have the cage's angular velocity of ω_c. For no skidding to occur in a bearing rotating at a constant speed, the axial deformation should be slightly increased by diminishing the radial deformation. The angular velocity of the cage becomes the dominant factor as to the determination of the proper deformations in the two directions. A rise in the angular velocity ω_c should apply a higher deformation in the axial direction to prevent the bearing from skidding. Since the threshold of skidding as shown in Eq. (42) was proposed on the basis of several empirical results, the validity of this criterion can be illustrated by choosing five points on each side of the threshold line of constant ω_c. Fig. 12 shows examples of all five points beneath the threshold line, with the cage's angular velocity set at 4000 rpm, and the deformation applied in the axial direction is 0.030 mm. In this figure, the values of Q_a/F_c varying with the position angle are shown for five radial deformations. The line for Q_a/F_c is equal to 10, which is the threshold of surface skidding. Apparently, all five

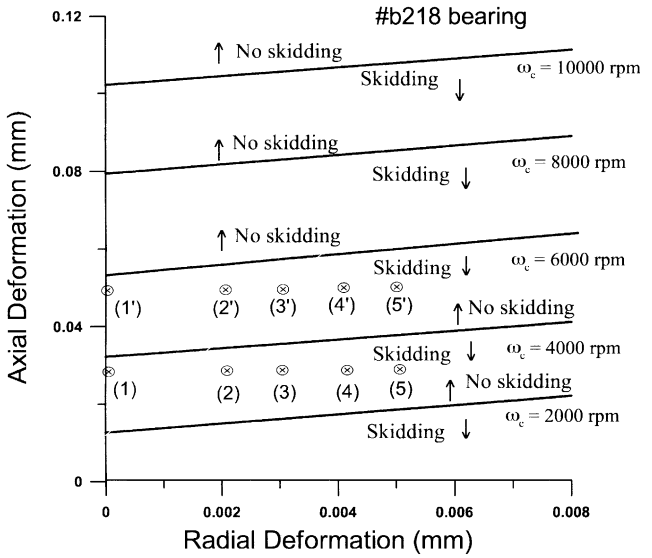

Fig. 11. The skidding criterion for the b218 ball bearing.

curves are either wholly or partly below the threshold line. That is, skidding occurs definitely for all five cases. As the axial deformation and the angular velocity of the cage are constant, increasing the radial deformation (thus the radial load) would reduce the possibility where skidding disappears. If the axial deformation is chosen such that four points are all above the threshold line of $\omega_c = 4000$ rpm (shown in Fig. 11), the Q_a/F_c values vary with the position angle of the bearing, as shown in Fig. 13. Here the axial deformation is increased to 0.045 mm. All four curves are

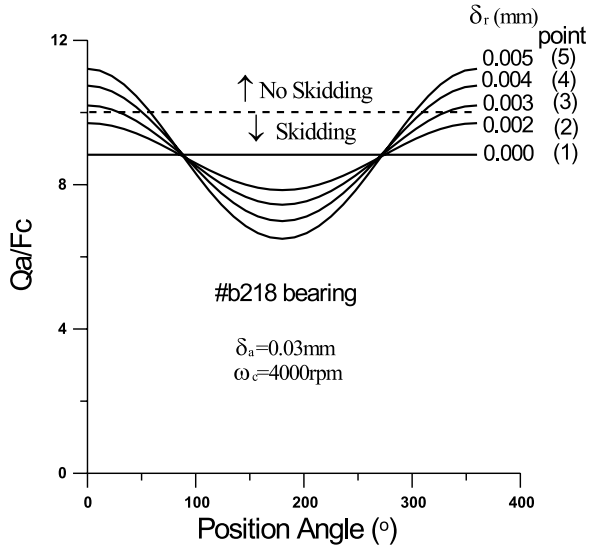

Fig. 12. The ratio Q_a/F_c varying with the bearing position angle under different radial deformations.

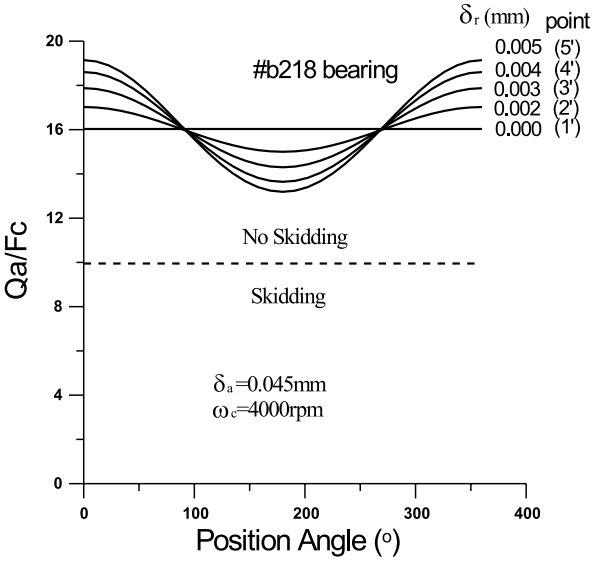

Fig. 13. The force ratio Q_a/F_c varying with the bearing position angle under different radial deformations.

located above the line of $Q_a/F_c = 10$; consequently, no skidding occurs. Proper reduction of the shaft diameter can effectively avoid skidding even when working at high angular velocities. However, if a finite value of the axial load is required, an appropriate choice of the bearing with a moderate value of the static-state contact angle (α^0) is needed in order to prevent the ball bearing from skidding. As Fig. 14 shows, skidding can possibly still be avoided by means of reducing the diameter of the shaft even when a high angular velocity is demanded.

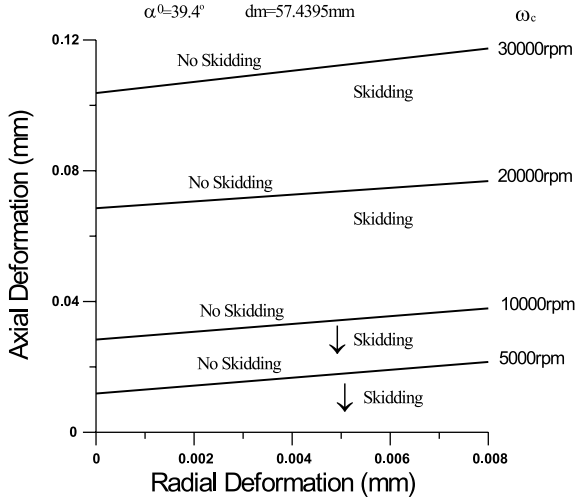

Fig. 14. The skidding criterion for the #7307 ball bearing at four different angular velocities of the cage.

3.4. The axial and radial stiffnesses

The variations of the axial load with bearing deformation in the axial direction at various angular velocities of the cage are shown in Fig. 15. The behavior of the bearing with a positive axial deformation is exactly opposite to that of a negative deformation. In the region with a negative δ_a, increasing the angular velocity of the cage elevates bearing stiffness in the axial direction, represented by the slope of a curve. Conversely, this bearing stiffness is lowered significantly by increasing the cage's angular velocity when a positive axial deformation is applied. It should be noticed that the curve for the angular velocity of the cage at 10 000 rpm largely lies in the region of $\delta_a < 0$; that is, the axial load applied to a bearing with the cage's angular velocity at 10 000 rpm is much higher than that required at relatively lower angular velocities when a positive bearing deformation (δ_a) is required. The radial loads created at the various angular velocities of the cage are shown in Fig. 16. If the system operates without axial deformation, increasing the angular velocity of the cage increases the bearing stiffness in the radial direction. As the axial deformation increases to 0.02 mm, the increase in the radial deformation under a constant radial load makes the bearing stiffness decrease in the radial direction as the cage's increases. As Fig. 16 shows, the application of a positive axial deformation causes a bearing with a higher angular velocity to have a lower stiffness increase in the radial direction.

From Figs. 15 and 16, the following conclusions can be drawn: the bearing stiffness in either the axial or the radial direction is decreased by increasing the cage's angular velocity when a positive deformation in the axial direction δ_a is applied. An increase in the radial deformation would decrease a bearing's stiffness in the axial direction, especially for a bearing operating at a low cage's angular velocity. However, the influence on the bearing's stiffness in the radial direction, due to a raise of the radial deformation, is negligibly small, whether an axial deformation is given or not.

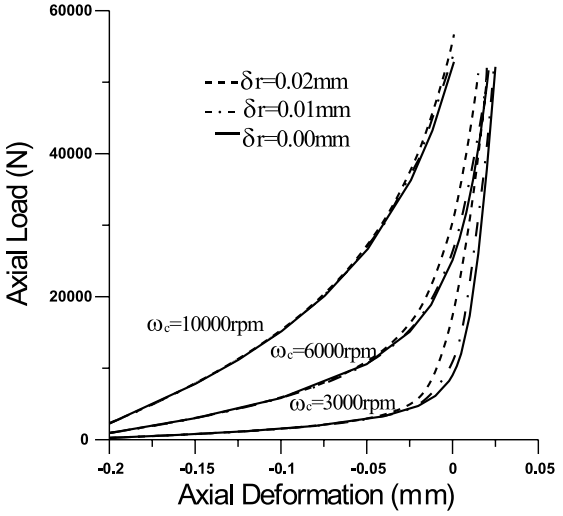

Fig. 15. Axial load vs. axial deformations of $\delta_r = 0$ mm, $\delta_r = 0.01$ mm and $\delta_r = 0.02$ mm at different cage's angular velocities.

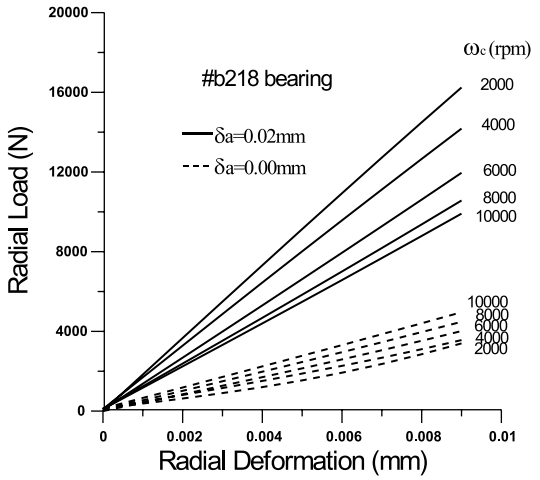

Fig. 16. Radial load vs. radial deformation of $\delta_a = 0$ mm and $\delta_a = 0.02$ mm at different cage's angular velocities.

4. Conclusions

1. The variation of the contact angle at either the inner or the outer raceways with the bearing position angle is affected greatly by the angular velocity of the cage. The difference between these two contact angles is enhanced by an increase of the cage's angular velocity resulting in different normal forces acting on the contact points; bearing stiffnesses in the axial and radial directions; and deformations required in the axial and radial directions to prevent a bearing from skidding.
2. The deformations applied in the radial and axial direction and the angular velocity of the cage form the controlling factors in the occurrence of skidding in a bearing. A more effective way to prevent a bearing from skidding at high angular velocities is to increase the deformation applied in the axial direction. That is the dominant factor in the choice of the axial deformation to avoid surface skidding.
3. Bearing stiffness in the axial direction is governed by the following parameters: the cage's angular velocity and the deformations applied in the radial and axial direction. Increasing the cage's angular velocity would decrease bearing stiffness significantly in the axial direction. If a positive axial deformation were applied, increasing the deformation in the radial direction, then the radial load would decrease the axial stiffness. Applying a positive deformation in the axial direction noticeably increases bearing stiffness in the radial direction. The bearing system with a lower angular velocity always has a higher stiffness in the radial direction.
4. Reduction in the shaft diameter can work in a considerably high angular velocity without bearing skidding when the contact angle α^0 is not too low.

Acknowledgements

The authors would like to thank the anonymous reviewers and Dr. terry E. Shoup, Dean School of Eng. Santa Clara University in USA for their constructive criticism and suggestions. In

particular, the authors would give our appreciation to one of them for his sincere helps on this research.

Appendix A

The sum and the difference of curvatures in a ball bearing are needed in order to obtain the normal loads on the ball. The sum of curvatures ρ is expressed as [10]:

$$\sum \rho = \frac{1}{r_{I1}} + \frac{1}{r_{I2}} + \frac{1}{r_{II1}} + \frac{1}{r_{II2}} \tag{A.1}$$

and the curvature difference $F(\rho)$ is expressed as [10]:

$$F(\rho) = \frac{(\rho_{I1} - \rho_{I2}) + (\rho_{II1} - \rho_{II2})}{\sum \rho}. \tag{A.2}$$

The parameters, r_{I1}, r_{I2}, r_{II1}, r_{II2}, ρ_{I1}, ρ_{I2}, ρ_{II1} and ρ_{II2} are given by the calculations in reference to the inner or outer raceways. If the inner raceway is considered, then

$$\begin{cases} r_{I1} = D/2, \\ r_{I2} = D/2, \\ r_{II1} = d_{\mathrm{i}}/2, \\ r_{II2} = r_{\mathrm{i}}. \end{cases} \quad \begin{cases} \rho_{I1} = 2/D, \\ \rho_{I2} = 2/D, \\ \rho_{II1} = 2/d_{\mathrm{i}}, \\ \rho_{II2} = -1/r_{\mathrm{i}}. \end{cases}$$

If the outer raceway is considered, then

$$\begin{cases} r_{I1} = D/2, \\ r_{I2} = D/2, \\ r_{II1} = d_{\mathrm{o}}/2, \\ r_{II2} = r_{\mathrm{o}}. \end{cases} \quad \begin{cases} \rho_{I1} = 2/D, \\ \rho_{I2} = 2/D, \\ \rho_{II1} = -2/d_{\mathrm{o}}, \\ \rho_{II2} = -1/r_{\mathrm{o}}. \end{cases}$$

Now, three dimensionless parameters are defined as:

$$\gamma = \frac{D\cos\alpha}{d_{\mathrm{m}}},$$

$$f_{\mathrm{o}} = \frac{r_{\mathrm{o}}}{D},$$

$$f_{\mathrm{i}} = \frac{r_{\mathrm{i}}}{D}.$$

Then, Eq. (A.1) for either the inner or the outer raceways is rewritten as:

$$\sum \rho_{\mathrm{i}} = \frac{1}{D}\left(4 - \frac{1}{f_{\mathrm{i}}} + \frac{2\gamma}{1-\gamma}\right), \tag{A.3a}$$

$$\sum \rho_{\mathrm{o}} = \frac{1}{D}\left(4 - \frac{1}{f_{\mathrm{o}}} - \frac{2\gamma}{1+\gamma}\right) \tag{A.3b}$$

and Eq. (A.2) for either the inner or the outer raceways is rewritten as:

$$F(\rho)_{\mathrm{i}} = \frac{\frac{2}{D}\left(\frac{\gamma}{1-\gamma}\right) + \left(\frac{1}{f_{\mathrm{i}}D}\right)}{\sum \rho_{\mathrm{i}}}, \tag{A.4a}$$

$$F(\rho)_{\mathrm{o}} = \frac{-\frac{2}{D}\left(\frac{\gamma}{1+\gamma}\right) + \left(\frac{1}{f_{\mathrm{o}}D}\right)}{\sum \rho_{\mathrm{i}}}. \tag{A.4b}$$

The elastic modulus K_{i} for the contact of a ball with the inner raceway is given as [10]:

$$K_{\mathrm{i}} = 1.084152 \times 10^6 \left(\sum \rho_{\mathrm{i}}\right)^{-0.5} (\delta_{\mathrm{i}}{}^*)^{-1.5} \tag{A.5a}$$

and for the contact of a ball with the outer raceway as:

$$K_{\mathrm{o}} = 1.084152 \times 10^6 \left(\sum \rho_{\mathrm{o}}\right)^{-0.5} (\delta_{\mathrm{o}}{}^*)^{-1.5}. \tag{A.5b}$$

In Eqs. (A.5a) and (A.5b), the parameter $\delta_{\mathrm{i}}{}^*$ and $\delta_{\mathrm{o}}{}^*$ can be attained from Table 2. if the values of $F(\rho)_{\mathrm{i}}$ and $F(\rho)_{\mathrm{o}}$ are available.

Table 2
The dimensionless contact parameters

$F(\rho)$	δ^*
0	1
0.1075	0.997
0.3204	0.9761
0.4795	0.9429
0.5916	0.9077
0.6716	0.8733
0.7332	0.8394
0.7948	0.7961
0.83595	0.7602
0.87366	0.7169
0.90999	0.6636
0.93657	0.6112
0.95738	0.5551
0.97290	0.4960
0.983797	0.4352
0.990902	0.3745
0.995112	0.3176
0.997300	0.2705
0.9981847	0.2427
0.9989156	0.2106
0.9994785	0.17167
0.9998527	0.11995
1	0

References

[1] A.B. Jones, Ball motion and sliding friction in ball bearing, ASME Trans. 81 (1959) 1–12.
[2] A.B. Jones, A general theory for elastically constrained ball and radial roller bearings under arbitrary load and speed conditions, ASME Trans. 82 (1960) 309–320.
[3] F. Hirano, Motion of a ball in angular-contact ball bearing, ASLE Trans. 8 (1965) 425–434.
[4] T.A. Harris, Ball motion in thrust loaded angular contact bearings with coulomb friction, J Lubr. Technol. Trans. ASME Ser. F 95 (1971) 106–108.
[5] T.A. Harris, An analytical method to predict skidding in thrust-loaded, angular-contact ball bearings, J. Lubr. Technol. Trans. ASME 93 (1971) 17–24.
[6] R.J. Boness, Minimum load requirements for the prevention of skidding in high speed thrust loaded ball bearings, J. Lubr. Technol. Trans. ASME 103 (1981) 35–39.
[7] P.K. Gupta, Dynamics of rolling-element bearings, J. Lubr. Technol. Trans. ASME 101 (1979) 312–326.
[8] J.V. Polawski, D.R. Atwell, M.J. Lubas, V. Odessky, Predicting steady-state temperature, life, skid, and film thickness in a greased preloaded hybrid ball bearing, ASME J. Eng. Gas Turbines Power 118 (1996) 443–448.
[9] N.T. Liao, J.F. Lin, A new method for the analysis of deformation and load in a ball bearing with variable contact angle, Trans. ASME J. Mech. Des. 123 (2001) 304–312.
[10] T.A. Harris, Rolling Bearing Analysis, 2nd ed, Wiley, New York, 1984.